Talanta 82 (2010) 1696–1700

Contents lists available at ScienceDirect

Talanta

journal homepage: www.elsevier.com/locate/talanta

Preparation of a new core–shell Ag@SiO_2 nanocomposite and its application for fluorescence enhancement

Liangqia Guo, Anhua Guan, Xiaolin Lin, Chunliang Zhang, Guonan Chen*

Ministry of Education Key Laboratory of Analysis and Detection for Food Safety, Fujian Provincial Key Laboratory of Analysis and Detection Technology for Food Safety, and Department of Chemistry, Fuzhou University, Fuzhou, Fujian 350002, China

ARTICLE INFO

Article history:
Received 24 May 2010
Received in revised form 19 July 2010
Accepted 22 July 2010
Available online 30 July 2010

Keywords:
Core–shell Ag@SiO_2 nanoparticle
Fluorescence enhancement
Metal-enhanced fluorescence
Rhodamine B isothiocyanate

ABSTRACT

Ag@SiO_2 nanoparticles with different shell thicknesses were synthesized via modified Stöber method. Rhodamine B isothiocyanate was covalently bound onto the surface of Ag@SiO_2 nanoparticles to form fluorescent core–shell Ag@SiO_2 nanocomposites. Effects of shell thickness on the fluorescence enhancement were examined using the corresponding nanobubbles prepared by cyanide etching as a control. The result showed that the fluorescence enhanced as the shell thickness increased till the distance between fluorophore and metal core reached about 75 nm with the optimal enhancement factor of ~5-folds. Further increasing of fluorophore–metal distance caused a decrease in the enhancement factor.

1. Introduction

Since Drexhage [1] found that a fluorophore near a metal film showed a dependence of its emissive lifetime on its distance from the metal surface, the influence of a metal on the emission of an oscillating dipole has been attracting great attention. It has been proved that fluorescence can be quenched when the fluorophore is in close proximity to a metal particle, but enhanced when the fluorophore is separated by a certain distance [2–4]. Such fluorescence enhancement phenomenon is defined as metal-enhanced fluorescence (MEF). MEF is based on the interactions of the excited-state fluorophores with the plasmon resonance of a metal particle and the enhancement scale depends on the particle size and shape [5,6]. MEF can increase the quantum yield and stability, reduce the lifetime of fluorescence [7] and broaden the transfer distance of fluorescence resonance energy transfer [8]. MEF is a useful technology and has been widely applied to increase the detection sensitivity of target molecule in biological assay [9–14].

The fundamental nature of MEF makes it be desirable to explore the effect of different metals on the characteristic of the fluorophores for many scientific and technological fields. To date, several metals have been used for MEF applications including silver [4,6,7,9–11,13], copper [5], gold [2,14], aluminium [15,16] and most recently zinc [17], chromium [18] and nickel [19]. In this regard, silver, gold, copper, zinc and chromium nanoparticles (NPs) were used for MEF in the visible wavelength region, while aluminium nanostructure films were shown to enhance the fluorescence in the UV and blue spectral region, respectively. Besides, nickel nanoparticle films can be used as substrate for near-IR MEF application. However, most of the MEF application to date have been performed on 2-dimensional planar surfaces, where glass microscope slides [4,6,7,9–14] and plastic [20,21] are used as the primary substrates that feature the nanostructures deposited using either wet-chemistry [4,6,9–11,13,14,20,21], electrochemistry [22] or lithography [22].

In 2004, Geddes [23] reported for the first time how SiO_2 coated silver colloid could be used as a solution based enhanced fluorescence sensing platform. Inspired by this promising result for solution-based MEF assay, they subsequently continued to develop a new class of fluorescent core–shell Ag@SiO_2 nanocomposites which were comprised of a ~130 nm silver core, a silica shell and fluorophores doped within silica shell and have demonstrated their applicability for metal-enhanced fluorescence [24,25] and single nanoparticle sensing [25]. Gerritsen [26] utilized both gold and silver as core metals for fluorescence enhancement study. Cheng and Xu [27] employed a SiO_2 spacer shell to vary the fluorophore–metal separation distance from 1 to 90 nm to study the fluorescence enhancement of fluorescein isothiocyanate by Ag NPs. Recently Boudreau investigated the effect of MEF on fluorescence self-quenching [28] and Förster resonance energy transfer [29]. These core–shell MEF-capable NPs provide several advantages. The SiO_2 shell can protect the fluorophores against collision quenching with the metal core, reduce the irreversible photodegradation under the incident light and offer the robustness, chemical inertness, and

* Corresponding author. Tel.: +86 0591 87893315; fax: +86 0591 83713866.
E-mail address: gnchen@fzu.edu.cn (G. Chen).

0039-9140/$ – see front matter © 2010 Elsevier B.V. All rights reserved.
doi:10.1016/j.talanta.2010.07.051

the versatility needed for the conjugation of biomolecules or fluorophores. Moreover, the mobility of these NPs is desirable for use in biosensing applications or for cell imaging work, as they are potentially injectable and silver and gold colloids are already widely used in medicine.

Here, we developed a new class of fluorescent core–shell $Ag@SiO_2$ nanocomposites for solution-based MEF research which comprised a silver core (~50 nm diameter), a silica-spacer shell of variable thickness, and a fluorophore-labeled shell. The size of silver particles 50 nm was chosen owing to its maximum enhancement efficiency of MEF for fluorophores near the surface of silver NPs [30]. Rhodamine B isothiocyanate (RITC) was chosen as the fluorophore because RITC was one of the common fluorescent labeling reagents. Moreover, RITC has outstanding brightness of fluorescence and less bleachable than fluorescein isothiocyanate [31,32], though its potential usefulness in core–shell based MEF has not hitherto been explored. The preparation of $Ag@SiO_2$ nanoparticles, fluorescent core–shell $Ag@SiO_2$ nanocomposites and the MEF phenomena were studied in detail. Our results showed that fluorescence enhanced as the shell thickness increased till the fluorophore RITC–metal distance reached 75 nm when the fluorescence reached the best enhancement effect of 5-folds.

2. Experimental

2.1. Chemicals

Tetraethyl orthosilicate (TEOS) and 3-aminopropyltriethoxysilane (APS) were purchased from ACROS. Silver nitrate was purchased from General Factory of Chemical Reagent of Shanghai, China. Sodium citrate, ethanol and isopropanol were purchased from Fuchen chemical reagent factory of Tianjin, China. Ammonium hydroxide was obtained from Sinopharm Chemical Reagent Co., Ltd. Rhodamine B isothiocyanate (RITC) was obtained from Shanghai Sangon Biological Engineering Technology & Services Co., Ltd. All chemicals used were analytical grade or above. 18.0 MΩ cm deionized water was used in all experiments.

2.2. Preparation of core–shell $Ag@SiO_2$ NPs

Core–shell $Ag@SiO_2$ NPs were obtained according to the method described in literature [33] with slight modification. The reaction scheme is presented in Fig. 1(A). Briefly, 9 mg $AgNO_3$ was dissolved in 49 mL H_2O and the solution was heated to boiling with vigorous stirring. 1 mL of 38.8 mmol/L trisodium citrate was added dropwise and the mixture was kept boiling for half an hour. The reaction solution was cooled down to room temperature. The prepared silver colloids were centrifuged at $66 \times g$ for 30 min to remove the larger size particles and the final volume was adjusted to 350 mL.

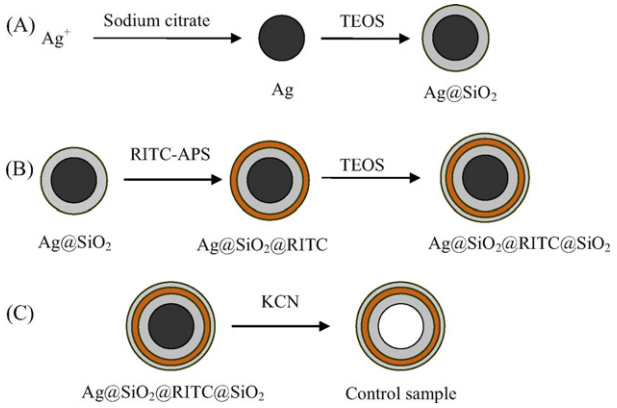

Fig. 1. Schematic representation of the preparation of core–shell $Ag@SiO_2$ NPs (A), RITC covalently binding to the silica shell of $Ag@SiO_2$ NPs (B), the preparation of control samples (C).

2 mL of the as-prepared Ag colloids were dispersed in 20 mL of isopropanol after stirring for 5 min. Then TEOS was added to the dispersion solution followed by the addition of 200 μL of ammonium hydroxide (28–30%) to initiate the formation of SiO_2 around the silver colloids. The reaction was kept at room temperature for 4 h under stirring. Different amount (5, 10, 15, 20, 25, 30, 40, 45, 50 μL) of TEOS was used in the reaction to control the thickness of the SiO_2 shell. The silica coated silver ($Ag@SiO_2$) core–shell NPs suspension was centrifuged at $9562 \times g$ for 10 min and washed with ethanol twice. The sediment was re-dispersed in 5 mL of ethanol and stored at 4 °C before further use.

2.3. Preparation of $Ag@SiO_2@RITC@SiO_2$ nanocomposites

The reaction scheme is presented in Fig. 1(B). 15 μL (0.064 mmol) of freshly distilled APS was added into 3 mL freshly distilled ethanol solution containing 10 mg (0.019 mmol) RITC. The reaction vessel was wrapped with aluminium foil to ensure a dark reaction environment. This reaction was kept for 24 h in room temperature under stirring. The result solution was referred to as APS–RITC.

3 mL core–shell $Ag@SiO_2$ NPs was dispersed in 7 mL newly distilled ethanol, then 10 μL APS–RITC was added after stirring for 5 min. The reaction was kept for 20 h in the dark and then 3 μL of TEOS and 200 μL ammonium hydroxide (28–30%) were added to initiate a second SiO_2 layer to against the fluorophores leakage. The reaction was kept for 3 h at room temperature under stirring. The suspension was purified by centrifugation at $9562 \times g$ for 10 min and the result sediment was washed with ethanol several times to remove the unbound fluorophores. The result product was re-dispersed in 5 mL ethanol and stored in 4 °C before use.

2.4. Preparation of control sample

In order to compare the fluorescence emission in a quantitative manner, control samples were prepared from the $Ag@SiO_2@RITC@SiO_2$ nanocomposites. The reaction scheme is presented in Fig. 1(C). 200 μL 1.0×10^{-6} mol/L KCN sodium bicarbonate buffer (pH 10.28) solution was added to 200 μL $Ag@SiO_2@RITC@SiO_2$ nanocomposites and stored for 2 h. The silver core could be etched by cyanide and hollow core–shell nanobubbles with different shell thickness were obtained.

2.5. Characterization of samples

The study of the composite NPs' size, morphology, and structure was performed by field emission transmission electron microscope (TEM, Model Tecnai G2 F20 S-TWIN 200KV, FEI Inc.). Steady-state fluorescence measurement was performed on a Varian Cary Eclipse spectrofluorometer and standard fused silica cuvette (optical path length of 1.0 cm) with right angle optical arrangement. The voltage of PMT was set at 800 V, which is the highest voltage to magnify the signal in the spectrofluorometer. If we take the measurement with 1 mm optical depth, the Rayleigh-scattering would be minished, at the same time the fluorescence intensities would be also reduced markedly. The result of the maximum for core–shell nanocomposites which was found at 10 μL of the added amount of APS–RITC were the same whether the measurements were taken with 1 mm optical depth or 1 cm optical depth. Taking the fluorescence intensities into account, 1 cm optical depth was used during the measurements.

The fluorescence spectra of $Ag@SiO_2@RITC@SiO_2$ nanocomposites and the control samples were excited at 540 nm in pH 10.28 sodium bicarbonate buffer solution. The slits of excitation and emission were fixed at 5 and 10 nm, respectively. The absorption spectra were measured on a UV–Vis spectrophotometer (model 2450, Shimadzu Inc.).

3. Results and discussion

3.1. Core–shell $Ag@SiO_2$ NPs

Well-dispersed spherical core–shell $Ag@SiO_2$ NPs were obtained using a standard citrate reduction along with an improved Stöber process [24,25,29,33]. Citrate-stabilized sliver NPs can be homogeneously coated with relatively thick silica shell by means of carefully tailoring the concentration of ammonia and TEOS in the diluted isopropanol solution without using a silane coupling agent 3-aminopropyltrimethoxysilane [23,27,34,35]. Ammonia could be added as a catalyst to speed up the hydrolysis of TEOS precursor. The formation of silica coating involved base-catalyzed hydrolysis of TEOS to generate silica sols, followed by nucleation and condensation of these sols onto the surface of silver NPs. Fig. 2(A) shows the absorbance and maximum peak of surface plasmon absorption of $Ag@SiO_2$ NPs during the sol–gel process. The surface plasmon resonance peak for silver NPs shifted toward longer wavelength as the thickness of the silica shell increased [24,25,36] on account of the increase in the local refractive index around the particles [36]. As expected, [34,36] addition of ammonia would promote damping of the surface plasmon band of silver NPs with time. This is because of aerial oxidation of Ag in the presence of NH_3 and dissolution in water as $Ag(NH_3)_2^+$ complex ions, which do not absorb in the visible wavelength range [34]. The reaction can be presented as

$$4Ag + 8NH_3 + O_2 + 2H_2O \rightarrow 4Ag(NH_3)_2^+ + 4OH^- \quad (1)$$

The oxidation rate of Ag correlates with the concentration of TEOS in the reaction. Fig. 2(B) shows the rate of Ag NPs oxidized by O_2 in the presence of different amounts of TEOS. The Ag NPs could be rapidly oxidized in the absence of TEOS, the intensity at the maximum was decreased to about one-third of the initial value after 4 h. When the concentration of TEOS increased, the rate of damping the surface plasmon band decreased [34]. This suggested that the more TEOS, the faster formation of SiO_2 shell, which protected the Ag core against the O_2 oxidation. When TEOS added was reached 50 μL, the formation of $Ag(NH_3)_2^+$ complex ions could be ignored (see Fig. 2(B) curve f).

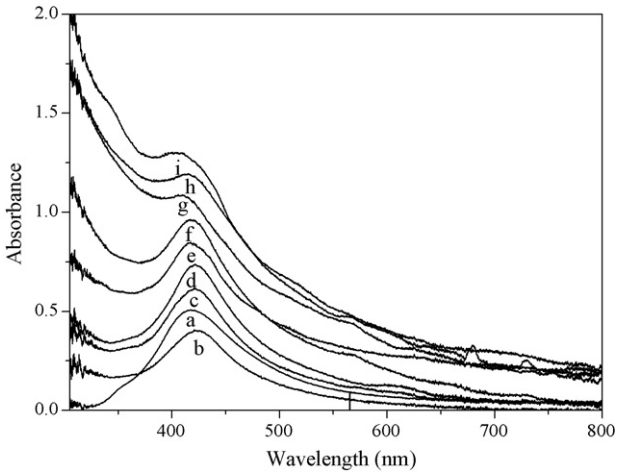

Fig. 3. UV–vis absorption spectra of citrate–Ag (a) and $Ag@SiO_2$ NPs with different shell thickness adjusted by the amount of TEOS (b) 10 μL, (c) 15 μL, (d) 20 μL, (e) 25 μL, (f) 30 μL, (g) 40 μL, (h) 45 μL, and (i) 50 μL.

The surface plasmon absorption in the visible wavelength region is very sensitive to both particle size and shape and to the properties of the surrounding medium [37]. Fig. 3 shows the UV–vis extinction spectra of citrate-protected silver NPs and $Ag@SiO_2$ NPs with different shell thickness. The surface plasmon bands of $Ag@SiO_2$ NPs where TEOS is less than 30 μL (Fig. 3(b–f)) were red-shifted with respect to the uncoated silver NPs (Fig. 3(a)) due to the increase of the local refractive index around the particles [36]. However, when the silica shell is sufficiently large, scattering becomes significant, resulting in a strong increase in the absorbance at shorter wavelength [36,37]. This effect promotes a blue shift of the surface plasmon band and a weakening in the apparent intensity of the plasmon band (Fig. 3(g–i)).

The surface plasmon resonance peak of silver NPs was 412 nm, and the diameter was about 50 ± 2 nm determined by TEM (Fig. 4(A)). The thickness of silica layer on the silver core can be regulated by the amount of TEOS and can be adjusted to optimize the metal–fluorophore distance for the next fluorescence enhancement study. Fig. 4(B–D) is typical TEM image of core–shell

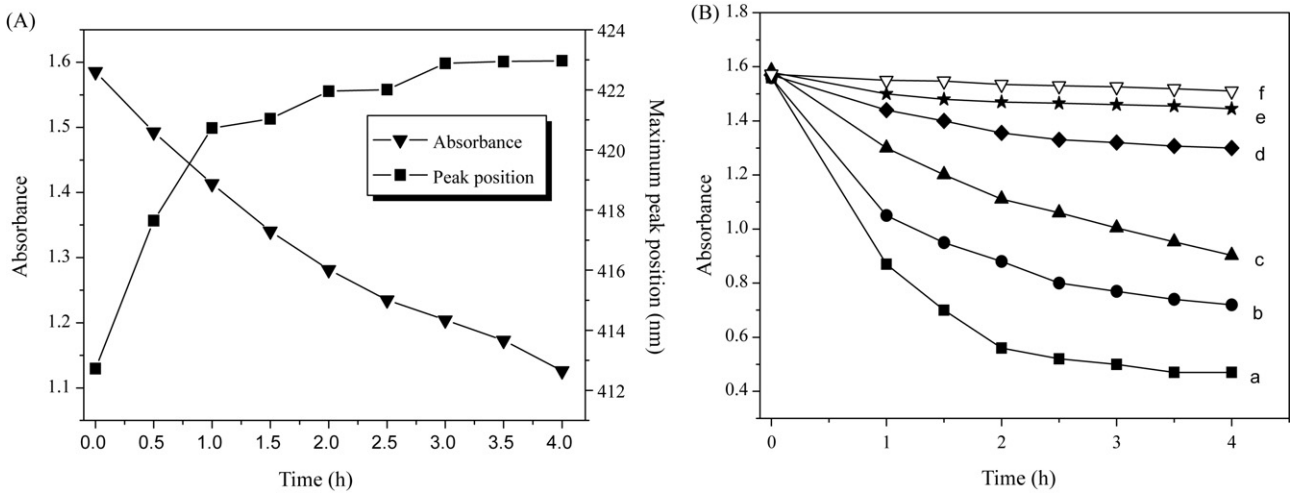

Fig. 2. (A) Time evolution of absorbance and maximum position of surface plasmon absorption of Ag NPs during the sol–gel process (TEOS: 10 μL). (B) Time evolution of absorbance of surface plasmon absorption of Ag NPs with the adding of difference amount of TEOS at the present of 200 μL of ammonium hydroxide. (a) 0 μL, (b) 10 μL, (c) 20 μL, (d) 30 μL, (e) 40 μL, and (f) 50 μL.

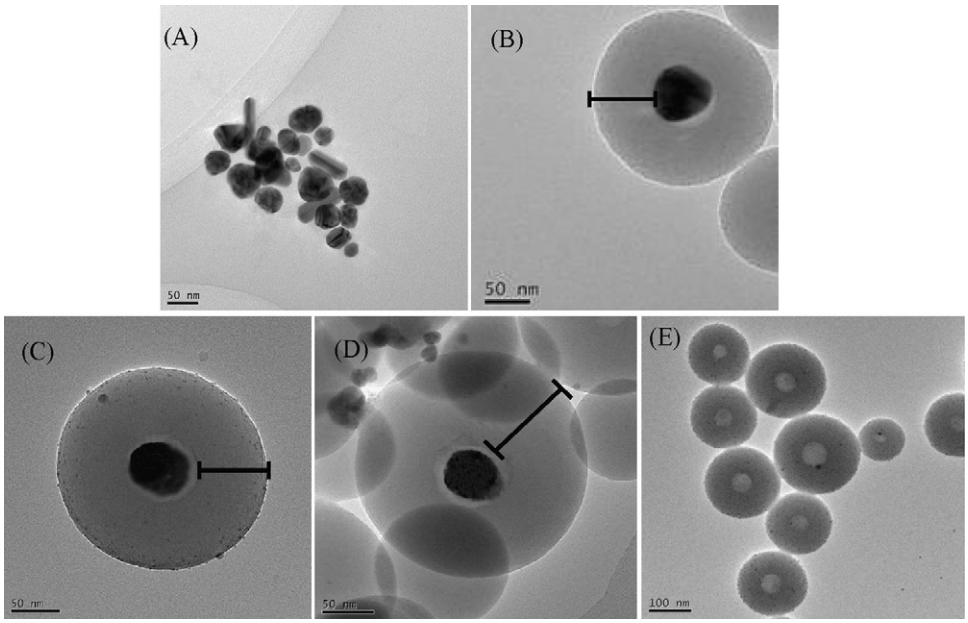

Fig. 4. TEM images of (A) silver particles, core–shell Ag@SiO_2 NPs with shell thickness of (B) 69 ± 2 nm, (C) 75 ± 2 nm, (D) 98 ± 2 nm, and (E) nanobubbles with silica shell thickness of 75 ± 2 nm.

Ag@SiO_2 NPs with the silica shell thickness of 69 ± 2, 75 ± 2 and 98 ± 2 nm when 10, 30 and 40 μL of TEOS are used, respectively. The fluorophore–metal distance was defined as the distance from the edge of the first SiO_2 layer to the edge of the Ag NPs.

3.2. Core–shell Ag@SiO_2@RITC@SiO_2 nanocomposites

The preparation of the RITC incorporated core–shell Ag@SiO_2@RITC@SiO_2 nanocomposites was similar to the strategy as described by Cheng and Xu [27]. We first synthesized an RITC-conjugated silane coupling agent to covalently bind the dye molecules onto the Ag@SiO_2 NPs, then a second silica shell layer was formed in order to prevent dyes leakage from the silica shell and ensure long-term stability of the NPs' luminescence. The dye RITC was covalently attached to the coupling agent APS by an addition reaction of the amine group with the isothiocyanate group (see Fig. 5).

Effect of RITC concentration on the fluorescence intensity of Ag@SiO_2@RITC@SiO_2 nanocomposites (all samples used here were with 75 nm silica shell thickness) was shown in Fig. 6. A slightly red shift of the fluorescence spectra was observed compared with free RITC ($\lambda_{Em}^{max} = 568$ nm) for the change in the environment of dye molecules after incorporation into the silica shell [38]. The fluorescence emission reached maximum for the nanocomposites with an amount of APS–RITC 10 μL. Beyond this dye concentration, a pronounced decrease in fluorescence intensity was observed. The number of dye molecules in the silica shell increases upon increasing the dye concentration. This leads to interactions between neighboring dye molecules, which lowers their excited state energy and produces a red shift in the spectra [28,29,38]. In our experiments these interactions also lead to significant self-quenching, which can be seen from the strong decrease in fluorescent intensity from S3 to S6. Thus S3 was used for further MEF study because it has the highest fluorescence intensity.

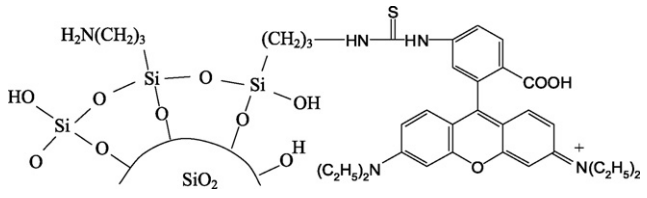

Fig. 5. Schematic representation of the RITC–APS coated particle surface of Ag@SiO_2 NPs.

3.3. Metal-enhanced fluorescence phenomena

To confirm the influence of the metal core on fluorescence emission, control samples (hollow core–shell nanobubbles) were prepared from fluorescent core–shell nanocomposites by dissolving the silver core with cyanide [25]. The metallic silver is attacked by cyanide in the presence of air, oxidized to $Ag(CN)_2^-$ [34] according to

$$4Ag + 8CN^- + O_2 + 2H_2O \rightarrow 4Ag(CN)_2^- + 4OH^- \quad (2)$$

Fig. 4(E) is the TEM image of the control samples, which validates that the silver core is removed away by virtue of the KCN etching. Fig. 7 shows the fluorescence emission intensity from Ag@SiO_2@RITC@SiO_2 nanocomposites with shell thickness of

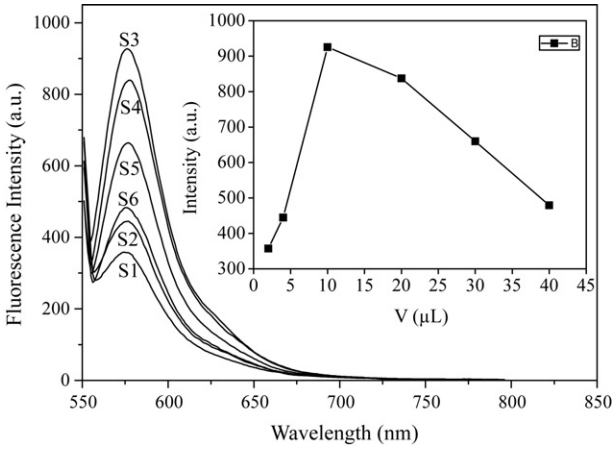

Fig. 6. Fluorescence spectra of Ag@SiO_2@RITC@SiO_2 by adding different amount of APS–RITC (from S1 to S6: 2, 4, 10, 20, 30 and 40 μL). Inset: effect of fluorescence intensity on the amount of APS–RITC added.

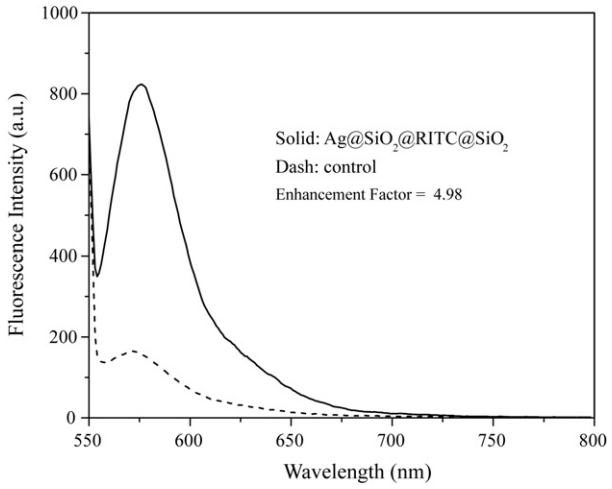

Fig. 7. Fluorescence emission spectra of $Ag@SiO_2@RITC@SiO_2$ nanocomposites (solid) and control sample (dot).

75 nm and from the corresponding fluorescent nanobubbles. The emission intensity of $Ag@SiO_2@RITC@SiO_2$ nanocomposites was approximately 5-folds higher than that of control samples. The fluorescence emission spectra of RITC were identical in both cases, indicating that the spectral properties of the fluorophores were retained.

Fig. 8 shows that the fluorescence enhancement of RITC is dependent on the shell thickness. For Ag–RITC nanocomposites, in which the isothiocyanate group (S=C=N–) of RITC is directly connected to Ag NPs by mixing Ag NPs with RITC directly, the fluorophore–metal distance is less than 1 nm [27]. The fluorescence of RITC is found to be quenched by a factor of ~4. This result is similar to the previous report [27]. The fluorescence quenching was attributed to resonant energy transfer from the fluorophores to the metal particle [27]. When the fluorophore–metal distance was separated by the first SiO_2 shell layer, the fluorescence intensity of RITC was found to be enhanced by MEF with the increasing of the shell thickness. The fluorescence enhancement factor is defined as the ratio of the fluorescence intensity of $Ag@SiO_2@RITC@SiO_2$ to the fluorescence intensity of the control. The optimal fluorescence enhancement with an enhancement factor of 4.98 occurred at a fluorophore–metal distance of 75 nm. Further increase of fluorophore–metal distance caused a decrease in the enhancement

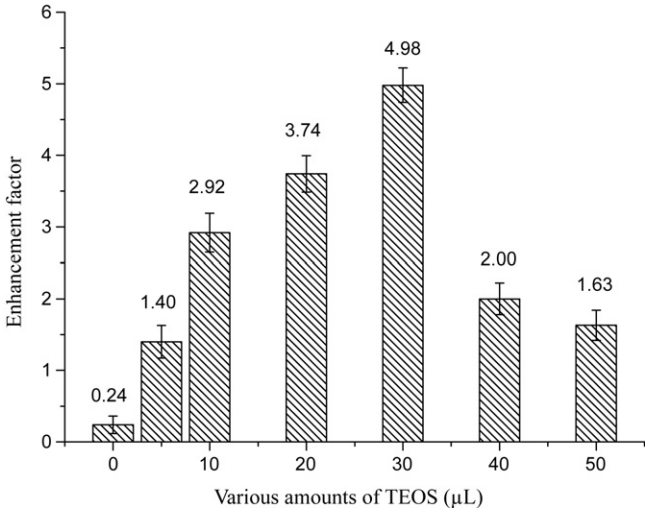

Fig. 8. Distance dependent fluorescent enhancement of the RITC by Ag NPs. (The shell thickness was adjusted by the amount of TEOS used during the preparation of $Ag@SiO_2$ NPs.)

factor. A fluorescence enhancement factor of 2.0 was still observed at a fluorophore–metal distance of 98 nm.

4. Conclusions

The RITC-labeled, silver core/silica shell nanocomposites were prepared to study the MEF phenomena. The use of a silica-spacer layer allows easy tuning of the dye–metal distance to large enough for the fluorescence enhancement to occur. For the silver core of 50 ± 2 nm, the optimal fluorescence enhancement with an enhancement factor ~5 was obtained when the fluorophore–metal distance was about 75 nm.

Acknowledgments

This project was financially supported by National Basic Research Program of China (No. 2010CB732403), the NSFC (50503006, 20735002, and 40940026) and Science Foundation of Fujian Province (2008J0149) of China.

References

[1] K.H. Drexhage, J. Lumin. 12 (1970) 693–701.
[2] J.R. Lakowicz, Anal. Biochem. 337 (2005) 171–194.
[3] O. Kulakovich, N. Strekal, A. Yaroshevich, S. Maskevich, S. Gaponenko, I. Nabiev, U. Woggon, M. Artemyev, Nano Lett. 2 (2002) 1449–1452.
[4] K. Ray, R. Badugu, J.R. Lakowicz, Langmuir 22 (2006) 8374–8378.
[5] Q. Darugar, W. Qian, M.A. El-Sayed, J. Phys. Chem. B 110 (2006) 143–149.
[6] K. Aslan, J.R. Lakowicz, C.D. Geddes, J. Phys. Chem. B 109 (2005) 6247–6251.
[7] J.R. Lakowicz, Y. Shen, S. D'Auria, J. Malicka, J. Fang, Z. Gryczynski, I. Gryczynski, Anal. Biochem. 301 (2002) 261–277.
[8] J. Malicka, I. Gryczynski, J. Kusba, J.R. Lakowicz, Biopolymers 70 (2003) 595–603.
[9] J. Malicka, I. Gryczynski, J.R. Lakowicz, Anal. Chem. 75 (2003) 4408–4414.
[10] J. Malicka, I. Gryczynski, J.R. Lakowicz, Biochem. Biophys. Res. Commun. 306 (2003) 213–218.
[11] K. Aslan, C.D. Geddes, Anal. Chem. 77 (2005) 8057–8067.
[12] K. Aslan, I. Gryczynski, J. Malicka, E. Matveeva, J.R. Lakowicz, C.D. Geddes, Curr. Opin. Biotechnol. 16 (2005) 55–62.
[13] K. Aslan, J. Huang, G.M. Wilson, C.D. Geddes, J. Am. Chem. Soc. 128 (2006) 4206–4207.
[14] W. Deng, K. Drozdowicz-Tomsia, D. Jin, E.M. Goldys, Anal. Chem. 81 (2009) 7248–7255.
[15] K. Ray, M.H. Chowdhury, J.R. Lakowicz, Anal. Chem. 79 (2007) 6480–6487.
[16] M.H. Chowdhury, K. Ray, S.K. Gray, J. Pond, J.R. Lakowicz, Anal. Chem. 81 (2009) 1397–1403.
[17] K. Aslan, M.J.R. Previte, Y. Zhang, C.D. Geddes, J. Phys. Chem. C 112 (2008) 18368–18375.
[18] R. Pribik, K. Aslan, Y. Zhang, C.D. Geddes, J. Phys. Chem. C 112 (2008) 17969–17973.
[19] Y. Zhang, A. Dragan, C.D. Geddes, J. Phys. Chem. C 113 (2009) 15811–15816.
[20] K. Aslan, R. Badugu, J.R. Lakowicz, C.D. Geddes, J. Fluoresc. 15 (2005) 99–104.
[21] K. Aslan, P. Holley, C.D. Geddes, J. Mater. Chem. 16 (2006) 2846–2857.
[22] C.D. Geddes, A. Parfenov, D. Roll, J. Fang, J.R. Lakowicz, Langmuir 19 (2003) 6236–6241.
[23] K. Aslan, J.R. Lakowicz, H. Szmacinski, C.D. Geddes, J. Fluoresc. 14 (2004) 677–679.
[24] K. Aslan, M. Wu, J.R. Lakowicz, C.D. Geddes, J. Fluoresc. 17 (2007) 127–131.
[25] K. Aslan, M. Wu, J.R. Lakowicz, C.D. Geddes, J. Am. Chem. Soc. 129 (2007) 1524–1525.
[26] O.G. Tovmachenko, C. Graf, D.J. van den Heuvel, A. van Blaaderen, H.C. Gerritsen, Adv. Mater. 18 (2006) 91–95.
[27] D. Cheng, Q.H. Xu, Chem. Commun. (2007) 248–250.
[28] M.L. Viger, L.S. Live, O.D. Therrien, D. Boudreau, Plasmonics 3 (2008) 33–40.
[29] M. Lessard-Viger, M. Rioux, L. Rainville, D. Boudreau, Nano Lett. 9 (2009) 3066–3071.
[30] J. Zhang, Y. Fu, M.H. Chowdhury, J.R. Lakowicz, J. Phys. Chem. C 112 (2008) 18–26.
[31] J.R. Lakowicz, Principles of Fluorescence Spectroscopy, Plenum Press, New York, 1984.
[32] R.C. Nairn, Fluorescent Protein Tracing, 4th ed., Churchill Livingstone, Edinburgh, 1976.
[33] S. Liu, Z. Zhang, M. Han, Anal. Chem. 77 (2005) 2595–2600.
[34] T. Ung, L.M. Liz-Marzán, P. Mulvaney, Langmuir 14 (1998) 3740–3748.
[35] T. Ung, L.M. Liz-Marzán, P. Mulvaney, J. Phys. Chem. B 103 (1999) 6770–6773.
[36] Y. Kobayashi, H. Katakami, E. Mine, D. Nagao, M. Konno, L.M. Liz-Marzán, J. Colloid Interface Sci. 283 (2005) 392–396.
[37] L.M. Liz-Marzn, M. Giersig, P. Mulvaney, Langmuir 12 (1996) 4329–4335.
[38] A. Imhof, M. Megens, J.J. Engelberts, D.T.N. de Lang, R. Sprik, W.L. Vos, J. Phys. Chem. B 103 (1999) 1408–1415.